JOURNAL OF CATALYSIS 96, 381–395 (1985)

Temperature-Programmed Reduction of $CoO-MoO_3/Al_2O_3$ Catalysts

P. ARNOLDY,[1] M. C. FRANKEN, B. SCHEFFER, AND J. A. MOULIJN

Institute for Chemical Technology, University of Amsterdam, Nieuwe Achtergracht 166, 1018 WV Amsterdam, The Netherlands

Received March 11, 1985

It is shown that temperature-programmed reduction (TPR) gives new information on the reducibility of $CoO-MoO_3/Al_2O_3$ catalysts. The reduction of Mo^{6+} surface species (monolayer and bilayer species) is not essentially affected by the presence of Co, whereas the reduction of Co^{2+} ions is strongly influenced by the presence of Mo. There appears to be a strong Co–Mo interaction at moderate Co contents: the reduction maximum for dispersed Co^{2+} ions decreases from around 1200 K, found for CoO/Al_2O_3, to 800–850 K for $CoO-MoO_3/Al_2O_3$. At high Co contents, Co_3O_4 crystallites and Co^{3+} ions in surface positions or in a crystalline $Co^{3+}-Al^{3+}$–oxide of proposed stoichiometry Co_3AlO_6 have been found in addition to the Co–Mo interaction phase. Solid-state diffusion of Co^{2+} ions starts already around 800 K, resulting in destruction of the Co–Mo interaction phase and in formation of subsurface Co^{2+} ions of low reducibility. By calcination at 1125 K, a significant loss of Mo takes place, while some $CoMoO_4$ microcrystallites are formed. Also some α-Al_2O_3 is formed, probably initiated by the presence of $CoMoO_4$.

INTRODUCTION

$CoO-MoO_3/Al_2O_3$ catalysts are commercially applied for hydrodesulfurization (HDS). They are an order of magnitude more active than both of the model systems CoO/Al_2O_3 and MoO_3/Al_2O_3 (*1, 2*). Therefore, close contact between Co and Mo atoms in the sulfided catalyst is generally supposed to be essential for obtaining high activity levels (*2–6*). One may wonder to what extent Co and Mo atoms are already in close contact in the oxidic precursor. Some authors have described the oxidic catalyst without Co–Mo interaction (*7, 8*). However, there is abundant evidence now that Co and Mo atoms do interact in the oxidic catalyst (*9–28*). Especially the influence of impregnation order of Co and Mo salts is obvious: when Mo is impregnated first, the Co dispersion is much higher (presence of less crystalline Co_3O_4), resulting in higher HDS activity (*11, 12, 19–21, 23, 26, 27, 29*). The origin and nature of Co–Mo interaction in the oxidic catalysts have not been elucidated in detail.

Reducibility can be used for characterizing oxidic structures. Literature data, however, strongly disagree with respect to the reducibility of $CoO-MoO_3/Al_2O_3$ catalysts, making more research on their reduction needed (*30*). Temperature-programmed reduction (TPR) has been shown to be a sensitive technique for studying reducibility (*31*) and has been applied successfully for the characterization of CoO/Al_2O_3 (*32, 33*) and MoO_3/Al_2O_3 (*34, 35*) catalysts. Especially the structure of CoO/Al_2O_3 appears to be complex (*32, 33*). Four different reduction regions can be present in TPR of CoO/Al_2O_3, which are assigned to four phases (I, II, III, and IV). Phase IV (reduction around 1200 K) is the main phase at moderate Co contents and consists either of surface Co^{2+} ions (IVA, low calcination temperatures) or of subsurface Co^{2+} ions (IVB and IVC, high calcination temperatures). With increasing Co content and after calculation at low temperatures, the phases I, II, and III appear. Phase I (reduction around 600 K) consists of Co_3O_4 crystallites. Phase II (reduction

[1] Present address: Koninklijke/Shell-Laboratorium, Badhuisweg 3, 1031 CM Amsterdam, The Netherlands.

0021-9517/85 $3.00

around 750 K) consists of Co^{3+} ions, in surface positions (IIA) or in a crystalline Co^{3+}–Al^{3+}–oxide of proposed stoichiometry Co_3AlO_6 (IIB). Phase III (reduction around 900 K) consists of surface Co^{2+} ions with less Al^{3+} ions in their surroundings than in the case of phase IVA.

In the present study, TPR of CoO–MoO_3/Al_2O_3 catalysts has been measured as a function of Co content and calcination temperature. These TPR results will be compared with those previously obtained for CoO/Al_2O_3 (*32, 33*). It will be shown that especially the reducibility of Co ions is strongly influenced by the presence of Mo. The TPR results of the present study will be correlated with HDS activity measurements in a separate study (*36*).

EXPERIMENTAL

a. Materials

Co_3O_4, $CoMoO_4$, $Co(NO_3)_2 \cdot 6H_2O$, and $(NH_4)_6Mo_7O_{24} \cdot 6H_2O$ were pro analysi chemicals. The preparation of $CoAl_2O_4$ has been described elsewhere (*32*). These compounds were X-ray diffraction (XRD)-pure, except for $CoMoO_4$ which was a mixture of the low- and high-temperature modifications a- and b-$CoMoO_4$ (ASTM 25-1434 and 21-868, respectively) (*37–39*). The Al_2O_3 support was a high-purity γ-Al_2O_3 (Ketjen 000-1.5E (CK 300); specific surface area 195 $m^2 g^{-1}$; pore volume 0.50 $cm^3 g^{-1}$; particle size 100–150 μm).

CoO–MoO_3/Al_2O_3 catalysts were prepared by pore volume impregnation of γ-Al_2O_3 with solutions of, successively, $(NH_4)_6Mo_7O_{24} \cdot 6H_2O$ and $Co(NO_3)_2 \cdot 6H_2O$ in demineralized H_2O. The impregnated solids were dried at atmospheric pressure in air, by gradually increasing the temperature from 325 to 380 K over a period of 3 h, followed by an isothermal period of 18 h at 380 K. After the first (Mo) impregnation, the resulting 10.4% MoO_3/Al_2O_3 catalyst was calcined in air at 795 K for 2 h (20-g samples; 700 μmol s^{-1}; internal diameter of the calcination tube 30 mm). After this calcination and the second (Co) impregnation step, the resulting CoO–MoO_3/Al_2O_3 catalysts were calcined in air again, at 675–1125 K for 2 h (2-g samples; 70 μmol s^{-1}; internal diameter of the calcination tube 10 mm). The MoO_3/Al_2O_3, without Co added, was also recalcined, in the same way as the CoO–MoO_3/Al_2O_3 catalysts. The Co additions were approximately 2, 4, and 10 g CoO per 100 g Al_2O_3. The catalysts will be designated by the number of metal atoms per nm^2 surface area, i.e., as Co(x)–Mo(y)/Al in which x is 0, 0.76, 1.61, or 4.07 Co atoms/nm^2 and y is always 2.49 Mo atoms/nm^2. These numbers refer to contents before calcination and are not corrected for changes of the Al_2O_3 surface area as a function of calcination temperature. It should be noted that after calcination at 1125 K the Mo content is much smaller than the nominal value of 2.49 at./nm^2 due to significant loss of Mo. Some of these catalysts have also been subjected to temperature-programmed sulfiding measurements, which have been published elsewhere (*40*).

b. X-Ray Diffraction (XRD)

XRD has been carried out in a Philips diffractometer PW 1050/25 using Co$K\alpha$ radiation. A Fe filter was applied to remove Co$K\beta$ radiation.

c. Diffuse Reflectance Spectroscopy (DRS)

DRS measurements (230–800 nm) have been carried out in a Cary 14 spectrometer. Samples were ground and painted on $MgCO_3$ surfaces. All DRS spectra were obtained against a $MgCO_3$ reference. The experimental $\log^{10}(I_0/I)$ data for catalysts were corrected for the small contribution of the unloaded Al_2O_3 support.

d. Temperature-Programmed Reduction (TPR)

The TPR equipment has been described in detail elsewhere (*32*). As reducing gas a 67% H_2/Ar high-purity gas mixture was used (flow rate 13 μmol s^{-1}; pressure 1.0

bar). The sample size was varied in the range 25–40 mg, in order to achieve a similar total H_2 consumption in each TPR experiment (ca. 85 μmol; calculated from reduction of Co^{2+} and Mo^{6+} to Co and Mo metal). The temperature was increased at a rate of 10 K min^{-1} up to the final temperature of 1250 K, which was maintained until the reduction was finished. H_2O, CO_2, and organics (except CH_4), which evolved during reduction, were trapped in 3A and 5A molecular sieve columns. H_2 consumption as well as CH_4, CO, and O_2 production was measured as a positive peak by means of a thermal conductivity detector (TCD). A flame ionization detector (FID) was used for CH_4 detection only. CH_4 and CO were retarded by the 5A molecular sieve (retardation times 2.4 and 3.7 min, respectively). Since the TPR patterns shown in Figs. 4–7 have not been corrected for these retardations, the CH_4 production peak is observed at a slightly too high temperature.

RESULTS

a. X-Ray Diffraction

The crystalline phases detected by XRD are summarized in Table 1. In no case have Mo-containing phases (e.g., MoO_3, $CoMoO_4$) been observed, whereas Co_3O_4 is found for the Co(4.07)–Mo(2.49)/Al cata-

TABLE 1

Characterization of $CoO-MoO_3/Al_2O_3$ Catalysts

Catalyst notation[a]	Calcination temperature (K)	Color	Crystalline phases (XRD)[b]	Mo content after calcination[c] (at./nm^2)
Mo(2.49)/Al	675	White	n.m.	2.49
	785	White	n.m.	2.49
	895	White	n.m.	2.49
	995	White	γ-/δ-Al_2O_3	2.49
	1125	White	δ-Al_2O_3	0.80
Co(0.76)–Mo(2.49)/Al	675	Light green	γ-Al_2O_3	2.49
	785	Light grey/blue	n.m.	2.49
	895	Light blue	γ-Al_2O_3, Co-Al-spinel	2.49
	995	Light blue	γ-/δ-Al_2O_3, Co-Al-spinel	2.49
	1125	Light blue	δ-Al_2O_3, α-Al_2O_3, Co-Al-spinel	0.92
Co(1.61)–Mo(2.49)/Al	675	Green	γ-Al_2O_3	2.49
	785	Green/blue	γ-Al_2O_3	2.49
	895	Blue	γ-Al_2O_3, Co-Al-spinel	2.49
	995	Blue	γ-/δ-Al_2O_3, Co-Al-spinel	2.49
	1125	Blue	δ-Al_2O_3, α-Al_2O_3, Co-Al-spinel	1.12
Co(4.07)–Mo(2.49)/Al	675	Dark green	γ-Al_2O_3, Co_3O_4	2.49
	785	Dark green	γ-Al_2O_3, Co_3O_4	2.49
	895	Dark green	γ-Al_2O_3, Co_3AlO_6, Co-Al-spinel	2.49
	995	Deep blue	γ-/δ-Al_2O_3, Co-Al-spinel	2.49
	1125	Deep blue	α-Al_2O_3, Co-Al-spinel	1.29

[a] Nominal Co and Mo contents (at./nm^2) are given in parentheses. The loss of Mo at 1125 K is not taken into account.

[b] n.m. = not measured. Co–Al–spinel = crystalline Co^{2+}–Al^{3+}–oxide with a Co^{2+} concentration much lower than that in $CoAl_2O_4$. Co_3AlO_6 = crystalline Co^{3+}–Al^{3+}–oxide of proposed stoichiometry Co_3AlO_6, with XRD lines coinciding with those of Co_3O_4 and distinguishable from Co_3O_4 by means of TPR.

[c] The Mo content after calcination at 1125 K, lowered by Mo loss, is calculated from quantitative TPR analysis, assuming that all Co is present as Co^{2+}.

lyst calcined at 675–785 K. For this high-loaded catalyst calcined at 895 K, XRD lines are still found at the same *d*-values as those related to Co_3O_4; here, however, these lines originate from crystallites of a Co^{3+}–Al^{3+}–oxide of proposed stoichiometry Co_3AlO_6, formed from Co_3O_4 by exchange of Co^{2+} and Al^{3+} ions between Co_3O_4 and γ-Al_2O_3 (*32*). α-Al_2O_3 is found in XRD after calcination at 1125 K, only for catalysts which contain both Co and Mo and in increasing amounts with increasing Co content.

Figure 1 shows the 2θ-value of the (440) reflection maximum as a function of calcination temperature. At elevated calcination temperatures, γ-Al_2O_3 (2θ-value of 79.6°) is transformed into either δ-Al_2O_3 (2θ-value of 79.9°) or a "Co–Al–spinel" (2θ-values below 79.6°). The latter is a Co^{2+}–Al^{3+}–oxide in which Co^{2+} ions occur in a much lower concentration than in $CoAl_2O_4$ (*32*). The tendency to form δ-Al_2O_3 is clearly suppressed by the presence of Co, to an increasing extent with increasing Co content, due to the alternative formation of stable Co–Al–spinel structures. δ-Al_2O_3 formation is observed after calcination above ca. 1000 K of Co(0–1.61)–Mo(2.49)/Al catalysts (line c). Co–Al–spinel structures are formed above ca. 800 K in the case of Co(0.76–1.61)–Mo(2.49)/Al and Co(4.07)–Mo(2.49)/Al catalysts (lines b and a, respectively). Line a is identical to the one previously obtained for Co(4.12)/Al catalysts (*32*). The smaller shift of the 2θ-value in line b with respect to line a is associated with the formation of more diluted Co–Al–spinel structures for catalysts with lower Co contents.

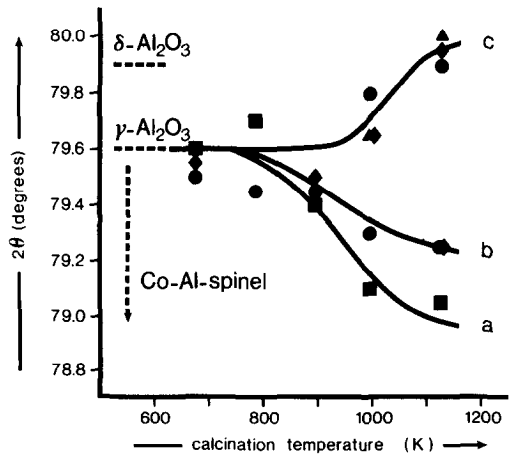

FIG. 1. The 2θ-value of the (440) reflection maximum as a function of calcination temperature of Co(x)–Mo(2.49)/Al catalysts. x = 0 at./nm² (triangles); x = 0.76 at./nm² (diamonds); x = 1.61 at./nm² (circles); x = 4.07 at./nm² (squares). Line a is identical with the one reported for Co(4.12)/Al in Ref. (*32*).

b. Diffuse Reflectance Spectroscopy

Colors are given in Table 1. The deep blue color of the Co(4.07)–Mo(2.49)/Al catalyst calcined at 995–1125 K is identical to the color observed for Co(4.12)/Al samples calcined in the same temperature range (*32*). Analysis of the DRS data gives more information than observation of the colors alone.

Figure 2 gives typical DRS spectra of CoO–MoO_3/Al_2O_3 catalysts. The Mo^{6+} absorption is only observed below 350 nm (charge transfer). In this range also a, much smaller, contribution due to charge transfer for Co ions is present. For dried catalysts (Figs. 2a and d), octahedrally surrounded Co^{2+} ions predominate (absorption around 530 nm). The triplet around 600 nm, due to the presence of tetrahedrally surrounded Co^{2+} ions, becomes more intense with increasing calcination temperature. Furthermore, absorption of Co^{2+} ions is present around 400 and 700–800 nm. The latter is only observed after calcination at 1125 K and is assigned to $CoMoO_4$ (see Discussion). Only for Co(4.07)–Mo(2.49)/Al samples calcined at low temperatures (Fig. 2e), the absorption due to the presence of Co^{3+} ions dominates the DRS spectrum between 350 and 800 nm. Quantitative analysis of the DRS spectra indicates that the Co^{3+} concentration on Co(0.76–1.61)–Mo(2.49)/Al catalysts is at least 100 times smaller than found for Co(4.07)–Mo(2.49)/Al in Fig. 2e.

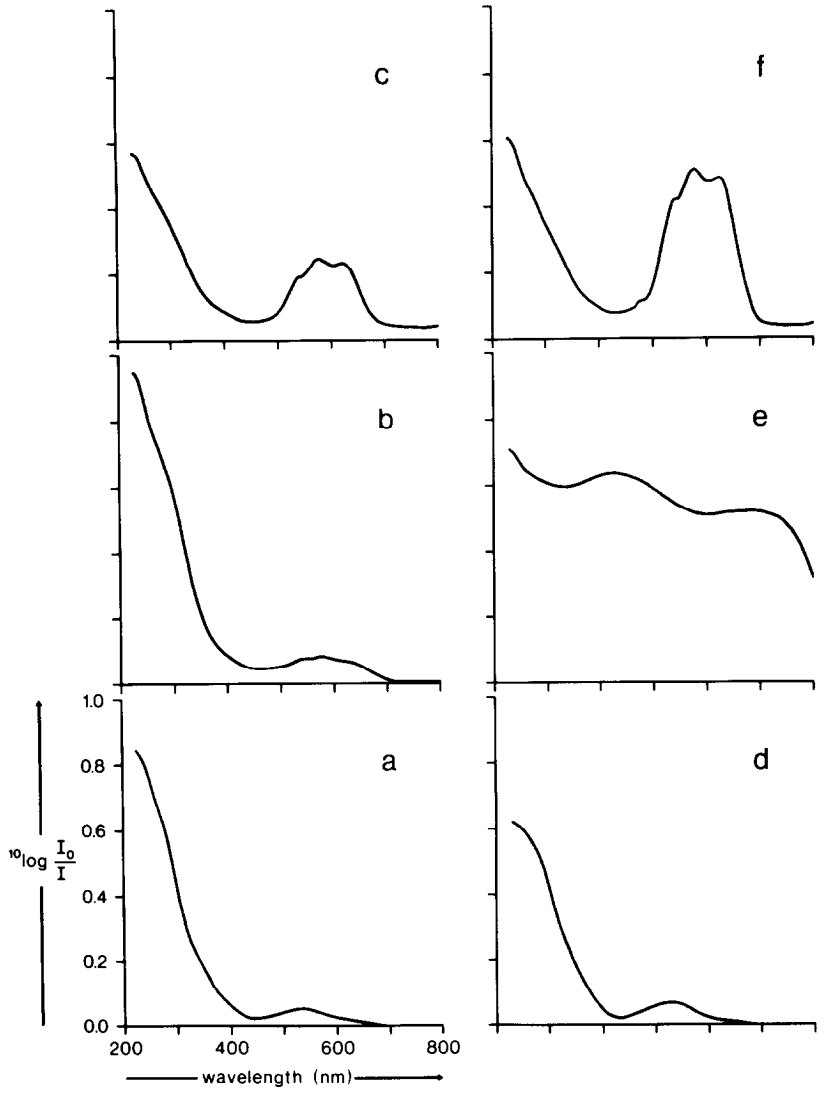

FIG. 2. Typical DRS spectra of Co(x)–Mo(2.49)/Al catalysts. These spectra have been corrected for the DRS spectrum of the unloaded γ-Al_2O_3. For all six spectra the axes are identical, viz. as shown in (a). (a, b, and c) x = 0.76 at./nm^2; (d, e, and f) x = 4.07 at./nm^2. The catalysts were not calcined (a and d), calcined at 785 K (b and e), or calcined at 1125 K (c and f).

c. Temperature-Programmed Reduction

Figure 3 shows TPR patterns of Co-containing crystalline compounds. The reducibility decreases in the order Co_3O_4–$CoMoO_4$–$CoAl_2O_4$. Especially the reduction of $CoMoO_4$ appears to occur in more than one step. In all cases, quantitative TPR analysis indicates that total reduction to Co and Mo metal takes place. No FID patterns are shown in Fig. 3, since the CH_4 production is negligible.

Figures 4–7 show TPR patterns of $CoO-MoO_3/Al_2O_3$ catalysts with various Co contents, as a function of calcination temperature. In Fig. 8 a survey is given of the position of the main TPR maxima (TCD detection) assigned to Co and Mo reduction, as a function of calcination temperature. Some TCD maxima are not shown, viz.

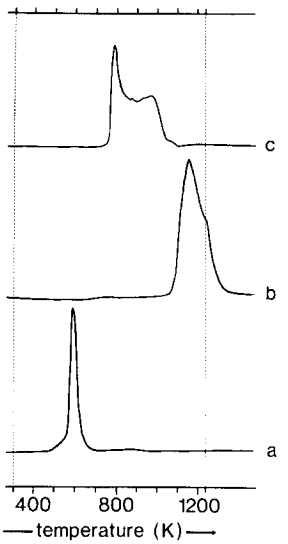

FIG. 3. TPR patterns at heating rate of 10 K min^{-1} of Co-containing crystalline compounds. (a) Co_3O_4; (b) $CoAl_2O_4$; (c) $CoMoO_4$. Only the TCD signals are given.

when the peak intensity is low and/or the TCD signal originates mainly from CH_4 production and the H_2 consumption belonging to this. Quantitative TPR analysis indicates that in most cases the TCD peak area, corrected for CH_4 production from adsorbed organics (*32, 41*), agrees with total reduction of Co^{2+} and Mo^{6+} to Co and Mo metal. Only for Co(4.07)–Mo(2.49)/Al catalysts calcined at 675–895 K, a 10% higher H_2 consumption was observed, which corresponds with a H_2 consumption of ca. 1.3 mol H_2/mol Co due to the presence of ca. 50% of the Co as Co^{3+}. For all samples calcined at 1125 K, the H_2 consumption is much lower than expected, obviously because of significant loss of Mo. In these cases TPR was used to calculate the Mo content after calcination at 1125 K (see Table 1). It appears that the Mo loss decreases significantly with increasing Co content. Temperature-programmed microbalance experiments confirmed the occurrence of Mo loss. It was found that sublimation of Mo oxides starts abruptly at 1110 K (He flow; heating rate 1 K min^{-1}) and continues after the temperature program for several hours at 1195 K.

The FID patterns obtained during TPR of MoO_3/Al_2O_3 (see Fig. 4) show that some CH_4 is formed over a broad temperature range, probably due to cracking of adsorbed organic impurities, whereas the FID patterns obtained during TPR of $CoO–MoO_3/Al_2O_3$ (see Figs. 5–7) show much more CH_4 production, which is associated

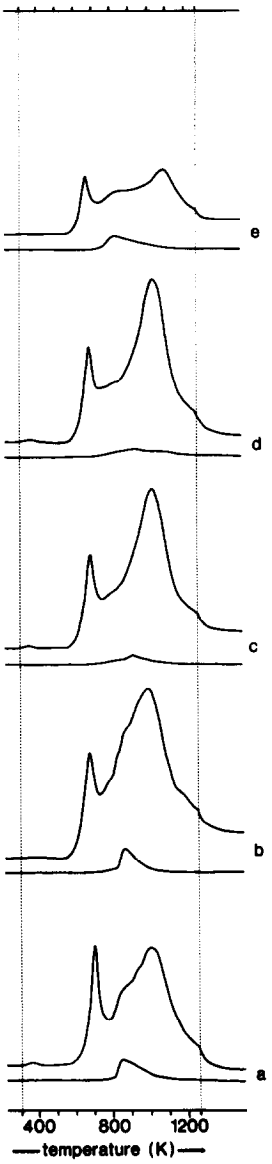

FIG. 4. TPR patterns (10 K min^{-1}) of Mo(2.49)/Al as a function of calcination temperature. (a) 675 K; (b) 785 K; (c) 895 K; (d) 995 K; (e) 1125 K. The upper and lower part of each pattern represent the TCD and FID signals, respectively.

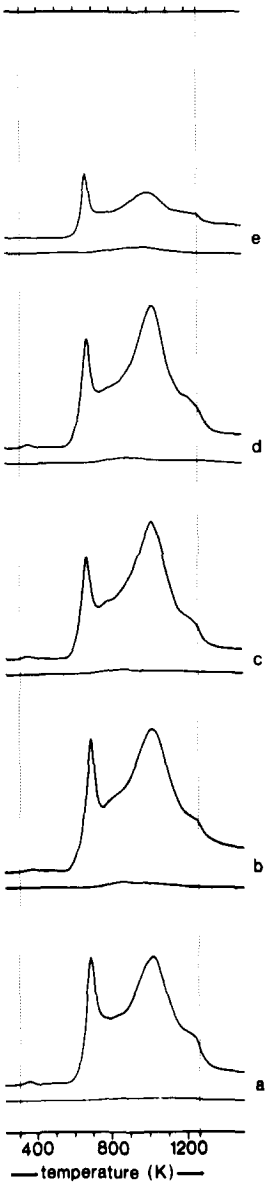

FIG. 5. TPR patterns (10 K min^{-1}) of Co(0.76–Mo(2.49)/Al as a function of calcination temperature. (a) 675 K; (b) 785 K; (c) 895 K; (d) 995 K: (e) 1125 K. The upper and lower part of each pattern represent the TCD and FID signals, respectively.

with reduction of these organic impurities (*32, 41*). In support of this, it has been found in separate experiments that the hydrogenation function (CO reduction) is poor and well-developed for reduced MoO_3/Al_2O_3 and $CoO-MoO_3/Al_2O_3$ catalysts, respectively. The start of the CH_4 production peaks in TPR is well-correlated with the start of formation of dispersed Co metal, which apparently catalyzes the reduction of organics (*32*). Therefore, the FID patterns can be used as an additional indication of the reduction temperature of Co species in $CoO-MoO_3/Al_2O_3$ catalysts.

TPR of MoO_3/Al_2O_3 (see Fig. 4) shows a two-peak pattern with maxima around 670

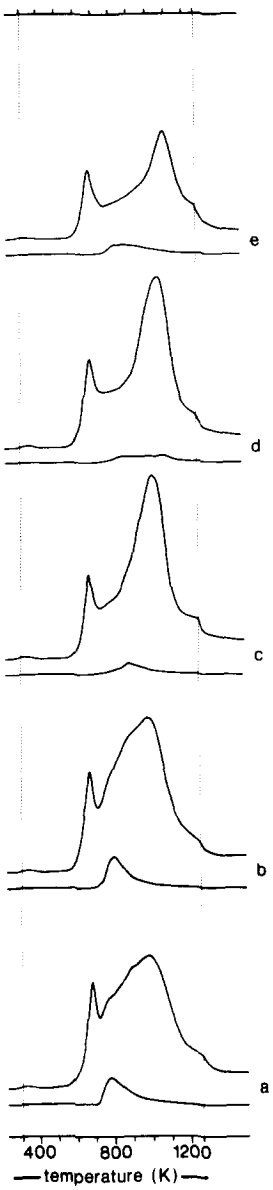

FIG. 6. TPR patterns (10 K min^{-1}), of Co(1.61)–Mo(2.49)/Al as a function of calcination temperature. (a) 675 K; (b) 785 K; (c) 895 K; (d) 995 K; (e) 1125 K. The upper and lower part of each pattern represent the TCD and FID signals, respectively.

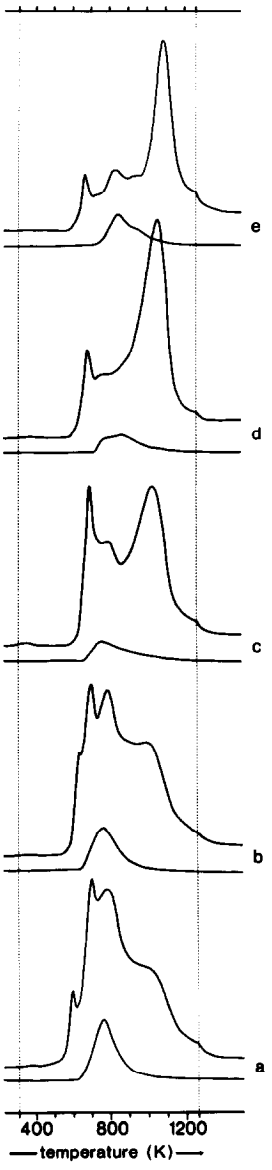

FIG. 7. TPR patterns (10 K min^{-1}) of Co(4.07)–Mo(2.49)/Al as a function of calcination temperature. (a) 675 K; (b) 785 K; (c) 895 K; (d) 995 K; (e) 1125 K. The upper and lower part of each pattern represent the TCD and FID signals, respectively.

K (Mo_I) and 1000 K (Mo_{II}). The kink in the TPR curve at the end of the temperature program shows that the reduction to Mo metal is not completed at that point; it is therefore possible that a small part of the reduction is missed due to the chosen end temperature. The low-temperature peak shifts from 680 to 660 K and decreases in intensity with increasing calcination temperature. The high-temperature peak does not shift, but increases slightly in intensity in the calcination temperature range 675–995 K and is much smaller after calcination at 1125 K as a result of Mo loss.

For $CoO–MoO_3/Al_2O_3$ catalysts (see Figs. 5–7), the fraction of the TPR pattern which is associated with reduction of Mo^{6+} ions is virtually the same as the TPR pattern found for MoO_3/Al_2O_3 (see Fig. 4), i.e., the Mo_I and Mo_{II} peaks are essentially present as in the Mo-only catalyst. The Mo_I

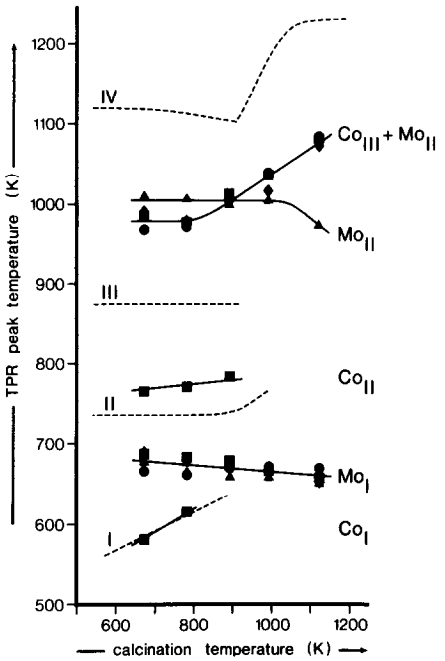

FIG. 8. The position of the main TPR peak maxima (TCD signals) for Co(x)–Mo(2.49)/Al as a function of calcination temperature. x = 0 at./nm^2 (triangles); x = 0.76 at./nm^2 (diamonds); x = 1.61 at./nm^2 (circles); x = 4.07 at./nm^2 (squares). For comparison, dotted lines are given which represent the position of the main TPR peak maxima (TCD signals, heating rate 10 K min^{-1}) for Co(4.12)/Al as a function of calcination temperature (copied from Ref. (*32*)). I, II, III, and IV represent different Co phases, which can be present on CoO/Al_2O_3 (see Introduction). Co_I, Co_{II}, Co_{III}, Mo_I, and Mo_{II} denote various reduction maxima present for Co and Mo reduction in the case of Co(x)–Mo(2.49)/Al.

peak shifts slightly as in the absence of Co (see Fig. 8). The reduction of Co species is traced in three temperature regions referred to as Co_I, Co_{II}, and Co_{III}. The Co_{III} and the Mo_{II} reduction peaks are always found together in the "Co_{III} + Mo_{II}" reduction peak (see Fig. 8). The shift of this peak is mainly caused by a sharp shift of the Co_{III} peak, independent of Co content, to higher temperatures for calcination temperatures above ca. 800 K. After calcination at 675–785 K, the Co_{III} + Mo_{II} maximum is found at a 20 K lower temperature than the Mo_{II} maximum in the absence of Co. In the light of the CH_4 production peaks around 800–850 K and the broadening of the Co_{III} + Mo_{II} peak to lower temperatures in Figs. 5a–b and 6a–b, it is concluded that this 20 K shift is caused by Co_{III} reduction around 800–850 K. Going to higher calcination temperatures, the Co_{III} + Mo_{II} peak shifts gradually from 980 to 1075 K. Especially after calcination at 1125 K (see Figs. 5e, 6e, and 7e), deconvolution into a (broad) Mo_{II} and a (sharp) Co_{III} reduction peak is possible. As a consequence, the position of the peak maximum at 1075 K has to be ascribed completely to Co reduction, the more so as significant fractions of Mo have been lost by calcination at 1125 K.

Besides the Co_{III} peak, some other Co reduction peaks can be distinguished:

—For Co(4.07)–Mo(2.49)/Al (see Figs. 7 and 8) peaks have been found around 600 K (Co_I; present after calcination at 675–785 K) and around 750 K (Co_{II}; present after calcination at 675–895 K).

—It is surprising that, independent of Co content, the CH_4 production, decreasing gradually in the calcination temperature range 675–995 K, clearly increases on going to the highest calcination temperature (1125 K). As the maximum of this FID peak is observed around 830 K in this case, it is concluded that at this temperature dispersed Co metal is present, probably due to reduction of $CoMoO_4$ microcrystallites (see Discussion, Section d).

DISCUSSION

a. Co-Containing Crystalline Compounds

Figure 3 shows that the reducibility decreases drastically in the order Co_3O_4–$CoMoO_4$–$CoAl_2O_4$. Clearly, the reducibility of Co ions depends on their surroundings to a large extent. It has already been reported that Al^{3+} ions polarize the more or less covalent Co–O bonds, making them more ionic and, consequently, stronger and less reducible (*32*). A similar polarization of Mo–O bonds by Al^{3+} ions has been proposed for explaining reduction and sulfiding results (*42*). We propose now that Mo^{6+} ions polarize Co–O bonds in the same way as Al^{3+} ions do, but to a much smaller extent.

Whereas Co_3O_4 and $CoAl_2O_4$ reduce essentially in one step (in the case of Co_3O_4, prereduction of Co^{3+} to Co^{2+} might be hidden on the low-temperature side of the TPR peak (*32*)), the reduction of $CoMoO_4$ appears to be more complicated. The $CoMoO_4$ TPR pattern can be deconvoluted into (at least) two peaks, namely, a first sharp peak at 880 K and a second broader peak around 950 K. The reduction starts around 750 K, in correspondence with the observation of slow and/or incomplete reduction at 675 K (*9, 24, 43*), at 775 K (*21, 37*), and at 750–835 K (*44*). The first TPR peak at 880 K probably corresponds with the reduction of $CoMoO_4$ to an equimolar mixture of $Co_2Mo_3O_8$ and Co_2MoO_4 (*39, 44*), since deconvolution of the TPR pattern shows that the H_2 consumption in the first peak is close to 1 mol H_2/mol $CoMoO_4$, which is needed for this conversion. The sharpness of the first peak indicates the presence of nucleation or autocatalysis as rate-determining step in reduction (*45*), in agreement with the induction period (acceleration) observed in isothermal reduction studies (*24, 39, 44*). Probably traces of Co metal are formed at the start of reduction (*43*), and these can act as catalytic centers for H_2 dissociation. In support of this, it was shown that addition of the easily reduc-

ible CoO to $CoMoO_4$ results in disappearance of the induction period (*46*). The second, broad peak corresponds with further reduction, from $Co_2Mo_3O_8$ and Co_2MoO_4 to Co and Mo metal. The broadness of the second peak is associated with the effect of H_2O on the reducibility of Mo oxide species, such as MoO_2 (*44, 47*). The fact that a mixture of a- and b-$CoMoO_4$ was used in the present study probably does not affect the TPR pattern, since it was shown that a- and b-$CoMoO_4$ have a comparable reducibility (*44*).

b. MoO_3/Al_2O_3

The reducibility of MoO_3/Al_2O_3 appears to be essentially independent of the calcination temperature (below 1110 K where Mo loss starts), in agreement with the literature (*21*). This suggests high stability of the structures in which the Mo^{6+} ions are present. The two-peak TPR pattern has been reported previously (*34, 35, 48–50*). The high-temperature peak (Mo_{II}) is assigned to reduction of tetrahedrally and octahedrally surrounded Mo^{6+} monolayer species, whereas the low-temperature peak (Mo_I) is related to reduction of octahedrally surrounded bilayer species (*34, 35*).

With increasing calcination temperature (675–995 K), some conversion of bilayer into monolayer species is observed. The same effect has been observed by recalcining air-exposed MoO_3/Al_2O_3 (*35*). Apparently, some additional Mo–O–Al linkages can be made by calcining, in increasing amounts with increasing calcination temperature, whereas they can be decomposed again by reaction with H_2O adsorbed from the atmosphere at room temperature (*35*). Also, the small shift of the Mo_I peak is associated with this bilayer–monolayer conversion, assuming that only those bilayer species are converted to monolayer species which reduce on the high-temperature side of the Mo_I peak (*35*).

The Mo loss at 1125 K, surprisingly, is related mainly to a decrease of the Mo_{II} peak, whereas the Mo_I peak is much less affected. The inverse was expected, considering the stronger interaction with the support in the case of the monolayer species (Mo_{II}). Two explanations arise.

1. Thermostable $Al_2(MoO_4)_3$ microcrystallites might be formed by calcination at 1125 K, which reduce in the Mo_I peak around 660 K. This explanation must be rejected, since the TPR peak maximum of $Al_2(MoO_4)_3$ has been observed only around 800 K (5 K/min) (*34*) and, moreover, Raman spectroscopy does not indicate the presence of $Al_2(MoO_4)_3$ after calcination at 1125 K (*51*).

2. More probably, at the high temperatures involved the sublimation of Mo oxides goes hand in hand with a decrease of the surface area. Both monolayer and bilayer species decompose, resulting in formation of volatile Mo oxides, which partly readsorb and reform monolayer and bilayer species on other parts of the surface. When the surface area decreases more rapidly than the Mo oxides are lost via the gas phase, the surface coverage, given in Mo atoms/nm^2, increases on the remaining surface. As a consequence of this increased surface coverage, an increased fraction of the Mo will be present as bilayer species (*35*).

c. CoO-MoO_3/Al_2O_3

TPR data on CoO–MoO_3/Al_2O_3, obtained by direct measurement of the H_2 concentration, have not been published before. In one case (*24*) TPR was measured by means of a microbalance, resulting in smooth curves of weight change as a function of reduction temperature. Apparently, the details observed by TPR in the present study were obscured by other phenomena, such as adsorption/desorption of H_2O and desorption, cracking or reduction of organic impurities. Also isothermal reduction measurements were carried out (*21, 24, 52–56*), which, however, were limited in their scope, since always one reduction temperature was chosen and, consequently, no picture was ob-

tained of the relative reducibility of all species present.

The reduction of Mo can be observed easily in TPR of $CoO-MoO_3/Al_2O_3$, since even at the highest Co content studied (4.07 at./nm^2) 65% of the TPR peak area is related to Mo reduction, when the calcination temperature remains below 1125 K. It appears that the position of the Mo_I and Mo_{II} peaks is essentially unaffected. Only after calcination at 1125 K, indications are present for some influence of Co on the Mo reducibility, by formation of $CoMoO_4$ (see Discussion, Section d). Therefore, it is concluded that for normal $CoO-MoO_3/Al_2O_3$ catalysts, with Mo impregnated first, Co does not affect the Mo reduction, in agreement with some reports in the literature (*21, 56*). The likewise reported inhibition of Mo reduction by Co (*21, 52, 55*) is restricted to the case of coimpregnated $CoO-MoO_3/Al_2O_3$ catalysts, probably due to the formation of $CoMoO_4$ at lower temperatures (*21*).

Indications for reduction of Co are found directly, from the TCD patterns, and indirectly, from the FID patterns (CH_4 production related to Co metal formation), as well as by comparison with TPR studies on the CoO/Al_2O_3 model catalysts (*32, 33*). Comparison with the TPR reduction maxima for CoO/Al_2O_3 (see Fig. 8) shows, for Co(4.07)–Mo(2.49)/Al catalysts, the presence of Co_3O_4 crystallites (Co_I = phase I; see Introduction) and of Co^{3+} ions, in surface positions or in a crystalline Co^{3+}–Al^{3+}–oxide of proposed stoichiometry Co_3AlO_6 (Co_{II} = phase IIA or IIB, respectively; see Introduction). It has been shown that the phases I and II decompose on going to higher calcination temperatures, due to reduction of Co^{3+} to Co^{2+} around 950 K and Co^{2+} diffusion (*32*). Co_3O_4 crystallites have not been found for the Co(0.76–1.61)–Mo(2.49)/Al catalysts (on the basis of TPR and DRS data), in contrast to the findings for CoO/Al_2O_3 catalysts with similar Co content prepared batchwise (*11, 21*), pointing to the often-reported increase of Co dispersion by the presence of Mo.

For all Co contents, reduction is found in a Co_{III} peak, which shifts from ca. 800–850 to 1075 K when the calcination temperature increases from ca. 800 to 1125 K. This Co_{III} reduction definitely does not correspond with the reduction of phase IV (see Fig. 8), whereas it was shown that phase IV predominates for CoO/Al_2O_3 with normally encountered moderate Co contents (ca. 1 at./nm^2) (*33*). Especially after calcination at low temperatures is the influence of Mo clear: whereas Co_{III} is observed around 800–850 K, reduction of phase IV has been found around 1110 K for Co(4.12)/Al catalysts (see Fig. 8) or even around 1240 K for Co(0.20–1.24)/Al catalysts (*33*), i.e., a difference of reduction temperature of ca. 300–400 K. Therefore, it is concluded that, for normal $CoO-MoO_3/Al_2O_3$ catalysts, Mo increases the Co reducibility drastically.

The influence of Mo on the Co reducibility after calcination below ca. 800 K can be explained as follows. Probably the Co^{2+} ions are bonded directly to the Mo structures via Co–O–Mo bridges. The presence of Mo^{6+} ions in the Co surroundings results in a decreased number of Al^{3+} neighbors. Because Al^{3+} ions polarize Co–O bonds much more than Mo^{6+} ions (see Discussion, Section a), the presence of Mo results in decreased polarization of the Co–O bonds and, consequently, in a much higher reducibility. In fact, the Co_{III} reduction maximum, after calcination below ca. 800 K, lies close to the one of the phases II and III found for CoO/Al_2O_3 (with ca. 4 and 7 Al^{3+} neighbors instead of ca. 10 in the case of phase IV (*32*)). Therefore, it is suggested that the Co_{III} reduction around 800–850 K corresponds to Co^{2+} ions which are coordinated to ca. 3 O–Al_2 ligands besides ca. 2 O–Mo ligands. These Co^{2+} ions might well be surrounded octahedrally, since this Co^{2+} coordination has been reported to occur in significant amounts (ca. 50% of the Co present), on the basis of magnetic susceptibility (*9–11, 29, 57*) and NO adsorption measurements (*27, 29*). The presence of

these octahedrally surrounded Co^{2+} ions appears to be related to the HDS activity of $CoO–MoO_3/Al_2O_3$ catalysts (*29, 57*). Quantitative analysis of the DRS spectra of the catalysts studied (see, e.g., Fig. 2) has confirmed that large fractions of the Co are present in octahedral coordination after calcination at 675–895 K, whereas the occurrence of this coordination declines with increasing calcination temperature within this temperature range. Also comparison of Figs. 2b and c shows qualitatively that the formation of tetrahedrally surrounded Co^{2+} ions is far from complete after calcination at 785 K.

The close proximity of Co and Mo ions explains the neutralizing effect of Co on the Mo Brønsted acidity (*13*). The coordination of this Co is affected by the gas-phase composition (*19, 57*), which emphasizes the exposure to the surface and suggests that the octahedral coordination is completed by some weakly adsorbed H_2O. EXAFS results show that this type of structure is completely disordered (*58–60*), in agreement with the present of such a less-well-defined, surface phase.

By calcination above ca. 800 K, solid-state diffusion of Co^{2+} ions occurs, as is evidenced by the shift of the Co_{III} reduction maximum from 800–850 to 1075 K and by XRD data showing the expansion of the Al_2O_3 lattice (see Fig. 1). The start of Co^{2+} diffusion around 800 K is in accordance with the literature (*13, 29*) and has been observed in a similar way for CoO/Al_2O_3 (*32*). Co^{2+} diffusion results in the formation of subsurface, tetrahedrally surrounded Co^{2+} ions (see Fig. 2). On the basis of DRS and XRD data, there is no reason to assume that these subsurface Co^{2+} ions differ from those present in CoO/Al_2O_3 catalysts calcined above ca. 800 K, to which is referred to as phase IVB and IVC (*32*). The difference in the position of the TPR maxima found for Co_{III} and phase IVB/IVC (see Fig. 8: 1075 and 1230 K, respectively) can be explained as follows. Subsurface Co^{2+} ions would reduce better in $CoO–MoO_3/Al_2O_3$ catalysts due to autocatalysis of the reduction by Co or Mo metal centers, formed at lower temperatures by reduction of Mo surface species (see Discussion, Section b) and $CoMoO_4$ microcrystallites (see Discussion, Section d). These metal centers would catalyze H_2 dissociation and, consequently, Co^{2+} ions, once diffused back to the surface, can be reduced directly without induction period. A similar acceleration of the attack of Co^{2+} ions reappearing at the surface has been observed in sulfiding of CoO/Al_2O_3 catalysts calcined at high temperatures (*33*).

d. The Influence of High Calcination Temperatures (1125 K)

Several specific results have been obtained for catalysts calcined at 1125 K, viz. formation of $CoMoO_4$ and α-Al_2O_3 and loss of Mo.

The CH_4 formation in TPR around 830 K after calcination at 1125 K, for all Co contents, points to the formation of a Co compound reducing at about 830 K. It is obvious that $CoMoO_4$ might be present, since it starts reducing around 850 K (see Fig. 3), is thermostable up to very high temperatures (*38, 39*) and is easily formed from separate Co and Mo phases (*9, 37, 39, 51*). The decreased loss of Mo in the presence of Co (see Table 1) might be associated with fixation of some gas-phase Mo oxides by Co^{2+} thus forming $CoMoO_4$ (*51*). If that is true, the decrease of the loss of Mo corresponds with 12–20% of the Co present as $CoMoO_4$ after calcination at 1125 K. XRD gives no evidence at all for $CoMoO_4$, which points to the presence of $CoMoO_4$ as clusters or microcrystallites (<3 nm). The presence of DRS absorption around 700–800 nm after calcination at 1125 K (see Fig. 2) also supports the $CoMoO_4$ formation. It should be noted that $CoMoO_4$ does not occur on normal $CoO–MoO_3/Al_2O_3$ catalysts (Mo impregnation first and calcination at low temperatures) (*7, 11, 18, 21, 43, 51, 59, 60*), whereas it is easily formed at high Co and

Mo contents or after coimpregnation (*9, 18, 21, 28, 53*). In one case (*53*), XRD lines due to $CoMoO_4$ (ASTM 21-868) were assigned incorrectly to MoO_3 (ASTM 5-508).

α-Al_2O_3 is only formed at 1125 K in the *combined* presence of Co and Mo on the Al_2O_3 surface; it has not been detected in the case of CoO/Al_2O_3 (*32*) or MoO_3/Al_2O_3 (the present study). α-Al_2O_3 formation between 1075 and 1175 K has been reported once previously (*61*), whereas some authors have not noticed it (*51, 62*).

Loss of Mo has been observed previously at 1125 K and even, in moist air, at 1025 K (*51*). The loss of Mo and the formation of α-Al_2O_3 and $CoMoO_4$ might be interconnected to some extent. The formation of $CoMoO_4$ is probably assisted by the volatility of the Mo oxides (see above). The formation and crystallization of α-Al_2O_3, only in the presence of both Co and Mo, is thought to be initiated by the $CoMoO_4$ microcrystallites formed. Probably those parts of the γ-/δ-Al_2O_3 surface which are depleted of Mo surface species due to Mo loss and contain only $CoMoO_4$ crystallites desintegrate, whereas the remaining parts are strongly stabilized by the presence of abundant amounts of Mo surface species.

e. Implications for HDS activity

TPR shows that the position of Co ions on the surface is strongly affected by the presence of Mo. This proves that there is intimate contact between Co and Mo in the $CoO-MoO_3/Al_2O_3$ catalysts. Therefore, essentially no rearrangements are necessary to establish good Co–Mo interaction in the sulfided catalyst. As has been concluded previously (*27*), a Co–Mo–O species is present which might well be the precursor for the HDS-active Co–Mo–S species.

The large difference in reducibility of Co^{2+} ions in CoO/Al_2O_3 and $CoO-MoO_3/Al_2O_3$ correlates well with the equally large difference in HDS activity found (*1, 2*). Moreover, it has been shown that NO adsorption on Co ions correlates well with HDS activity (*27*). Therefore, it is proposed that high HDS activity is associated mainly with Co sites. This is supported by the higher HDS activity for Co with respect to Mo in the case of carbon-supported catalysts (*63*). Consequently, the role of Mo is thought to be secondary, although still very important; Mo might be, in the oxidic as well as in the sulfided state, a promoter for HDS activity of Co sites, since Mo modifies the Al_2O_3 support to such an extent that the Co–support interaction is diminished strongly, resulting in less-polarized, more HDS-active Co in Co–Mo–S-type species.

The solid-state diffusion of Co^{2+} ions above 800 K is supposed to influence the HDS activity, since the latter is related to the presence of surface Co species. Indeed, it has been found that the calcination temperature affects the HDS activity of $CoO-MoO_3/Al_2O_3$ in the temperature range 775–975 K (*13, 29*), although the negative influence of calcination temperature is smaller than expected. In a separate study (*36*) HDS activity measurements for the catalysts studied will be correlated with the present TPR results.

CONCLUSIONS

1. The present TPR results give new information on the reduction of Co and Mo ions in $CoO-MoO_3/Al_2O_3$ catalysts. Besides the TCD pattern (H_2 consumption mainly) also the FID pattern (CH_4 production due to reduction of organic impurities) gives information on the reduction temperatures for Co species.

2. The reduction of Mo surface species (monolayer and bilayer Mo^{6+} species) is not essentially affected by the presence of Co, independent of Co content and calcination temperature. Only at very high calcination temperatures (1125 K) is evidence found for formation of microcrystalline $CoMoO_4$.

3. For $CoO-MoO_3/Al_2O_3$ catalysts with moderate Co content, calcined below 800 K, the reduction of Co^{2+} ions is drastically influenced by the presence of Mo; the reduction maximum due to Co reduction

shifts from ca. 1200 K for CoO/Al_2O_3 to 800–850 K for $CoO–MoO_3/Al_2O_3$, showing intimate Co–Mo contact. A Co–Mo–O precursor phase for the HDS-active Co–Mo–S species is suggested. It is proposed that Co, in fact, is the most HDS-active metal, whereas the major role of Mo is the promoting of Co HDS activity by decreasing the interaction between Co ions and the Al_2O_3 support.

4. For $CoO–MoO_3/Al_2O_3$ catalysts with high Co content, calcined below 800 K, also other Co phases are present besides the Co–Mo–O phase, viz. crystalline Co_3O_4 and Co^{3+} ions, in surface positions or in a crystalline $Co^{3+}–Al^{3+}$–oxide of proposed stoichiometry Co_3AlO_6.

5. For $CoO–MoO_3/Al_2O_3$ catalysts, independent of Co content, subsurface Co^{2+} ions are formed by calcining at temperatures above 800 K. This leads to gradual destruction of the Co–Mo interaction.

6. Calcination at 1125 K leads to a significant Mo loss, which is suppressed slightly by the presence of Co, because of some formation of $CoMoO_4$ microcrystallites. α-Al_2O_3 is formed at 1125 K, but only when both Co and Mo are present; the $CoMoO_4$ crystallites might initiate the α-Al_2O_3 formation.

ACKNOWLEDGMENTS

This study was supported by the Netherlands Foundation for Chemical Research (SON) with financial aid from the Netherlands Organization for the Advancement of Pure Research (ZWO). Thanks are due to Dr. B. Koch and Mr. W. Molleman (University of Amsterdam) for the XRD measurements and to Mr. A. Terpstra (University of Amsterdam) for the use of the DRS apparatus.

REFERENCES

1. de Beer, V. H. J., van Sint Fiet, T. H. M., van der Steen, G. H. A. M., Zwaga, A. C., and Schuit, G. C. A., *J. Catal.* **35,** 297 (1974).
2. Wivel, C., Candia, R., Clausen, B. S., Mørup, S., and Topsøe, H., *J. Catal.* **68,** 453 (1981).
3. Farragher, A. L., and Cossee, P., *in* "Proceedings, 5th International Congress on Catalysis, Palm Beach, 1972" (J. Hightower, Ed.), p. 1301. North-Holland, Amsterdam, 1973.
4. de Beer, V. H. J., and Schuit, G. C. A., *in* "Preparation of Catalysts" (B. Delmon, P. A. Jacobs, and G. Poncelet, Eds.), p. 343. Elsevier, Amsterdam, 1976.
5. Topsøe, H., Clausen, B. S., Candia, R., Wivel, C., and Mørup, S., *J. Catal.* **68,** 433 (1981).
6. Chianelli, R. R., Pecoraro, T. A., Halbert, T. R., Pan, W. H., and Stiefel, E. I., *J. Catal.* **86,** 226 (1984).
7. Lipsch, J. M. J. G., and Schuit, G. C. A., *J. Catal.* **15,** 174 (1969).
8. Topsøe, H., Clausen, B. S., Burriesci, N., Candia, R., and Mørup, S., *in* "Preparation of Catalysts II" (B. Delmon, P. Grange, P. A. Jacobs, and G. Poncelet, Eds.), p. 479. Elsevier, Amsterdam, 1979.
9. Richardson, J. T., *Ind. Eng. Chem. Fundam.* **3,** 154 (1964).
10. Ashley, J. H., and Mitchell, P. C. H., *J. Chem. Soc. A,* 2730 (1969).
11. Lo Jacono, M., Cimino, A., and Schuit, G. C. A., *Gazz. Chim. Ital.* **103,** 1281 (1973).
12. Lo Jacono, M., Verbeek, J. L., and Schuit, G. C. A., *J. Catal.* **29,** 463 (1973).
13. Moné, R., *in* "Preparation of Catalysts" (B. Delmon, P. A. Jacobs, and G. Poncelet, Eds.), p. 381. Elsevier, Amsterdam, 1976.
14. Grimblot, J., and Bonnelle, J. P., *J. Electron Spectrosc. Relat. Phenom.* **9,** 449 (1976).
15. de Beer, V. H. J., Bevelander, C., van Sint Fiet, T. H. M., Werter, P. G. A. J., and Amberg, C. H., *J. Catal.* **43,** 68 (1976).
16. Brown, F. R., and Makovsky, L. E., *Appl. Spectrosc.* **31,** 44 (1977).
17. Okamoto, Y., Nakano, H., Shimokawa, T., Imanaka, T., and Teranishi, S., *J. Catal.* **50,** 447 (1977).
18. Medema, J., van Stam, C., de Beer, V. H. J., Konings, A. J. A., and Koningsberger, D. C., *J. Catal.* **53,** 386 (1978).
19. Ratnasamy, P., and Knözinger, H., *J. Catal.* **54,** 155 (1978).
20. Delmon, B., *in* "Proceedings, 3rd International Conference on the Chemistry and Uses of Molybdenum" (H. F. Barry and P. C. H. Mitchell, Eds.), p. 73. Climax Molybdenum Co., Ann Arbor, Michigan, 1979.
21. Chung, K. S., and Massoth, F. E., *J. Catal.* **64,** 320 (1980).
22. Chung, K. S., and Massoth, F. E., *J. Catal.* **64,** 332 (1980).
23. Gajardo, P., Grange, P., and Delmon, B., *J. Catal.* **63,** 201 (1980).
24. Gajardo, P., Grange, P., and Delmon, B., *J. Chem. Soc. Faraday Trans 1* **76,** 929 (1980).
25. Topsøe, N. Y., *J. Catal.* **64,** 235 (1980).
26. Breysse, M., Bennett, B. A., Chadwick, D., and Vrinat, M., *Bull. Soc. Chim. Belg.* **90,** 1271 (1981).

27. Topsøe, N. Y., and Topsøe, H., *J. Catal.* **77,** 293 (1982).
28. Yerofeyev, V. I., and Kaletchits, I. V., *J. Catal.* **86,** 55 (1984).
29. Candia, R., Topsøe, N. Y., Clausen, B. S., Wivel, C., Nevald, R., and Mørup, S., *in* "Proceedings, 4th International Conference on the Chemistry and Uses of Molybdenum" (H. F. Barry and P. C. H. Mitchell, Eds.), p. 374. Climax Molybdenum Co., Ann Arbor, Michigan, 1982.
30. Massoth, F. E., "Advances in Catalysis," Vol. 27, p. 265. Academic Press, New York, 1978.
31. Hurst, N. W., Gentry, S. J., Jones, A., and McNicol, B. D., *Catal. Rev.* **24,** 233 (1982).
32. Arnoldy, P., and Moulijn, J. A., *J. Catal.* **93,** 38 (1985).
33. Arnoldy, P., de Booys, J. L., Scheffer, B., and Moulijn, J. A., *J. Catal.* **96,** 122 (1985).
34. Thomas, R., de Beer, V. H. J., and Moulijn, J. A., *Bull. Soc. Chim. Belg.* **90,** 1349 (1982).
35. Arnoldy, P., de Jonge, J. C. M., Wimmers, O. J., and Moulijn, J. A., submitted for publication.
36. Scheffer, B., van Oers, E. M., Arnoldy, P., de Beer, V. H. J., and Moulijn, J.A., in press.
37. Boutry, P., Daumas, J. C., Montarnal, R., Courtine, P., and Pannetier, G., *Bull. Soc. Chim. Fr.,* 4811 (1968).
38. Lipsch, J. M. J. G., and Schuit, G. C. A., *J. Catal.* **15,** 163 (1969).
39. Haber, J., *J. Less-Common Met.* **36,** 277 (1974).
40. Scheffer, B., de Jonge, J. C. M., Arnoldy, P., and Moulijn, J. A., *Bull. Soc. Chim. Belg.* **93,** 751 (1984).
41. Arnoldy, P., van Oers, E. M., Bruinsma, O. S. L., de Beer, V. H. J., and Moulijn, J. A., *J. Catal.* **93,** 231 (1985).
42. Arnoldy, P., van den Heijkant, J. A. M., de Bok, G. D., and Moulijn, J. A., *J. Catal.* **92,** 35 (1985).
43. Cimino, A., and De Angelis, B. A., *J. Catal.* **36,** 11 (1975).
44. Haber, J., and Janas, J., *in* "Reaction Kinetics in Heterogeneous Chemical Systems" (P. Barret, Ed.), p. 737. Elsevier, Amsterdam, 1975.
45. Wimmers, O. J., Arnoldy, P., and Moulijn, J. A., submitted for publication.
46. Haber, J., *in* "Proceedings, 2nd International Conference on the Chemistry and Uses of Molybdenum" (H. F. Barry and P. C. H. Mitchell, Eds.), p. 119. Climax Molybdenum Co., Ann Arbor, Michigan, 1976.
47. Arnoldy, P., de Jonge, J. C. M., and Moulijn, J. A., *J. Phys. Chem.,* in press.
48. Holm, V. C. F., and Clark, A., *J. Catal.* **11,** 305 (1968).
49. Yao, H. C., *J. Catal.* **70,** 440 (1981).
50. Hall, W. K., *in* "Proceedings, 4th International Conference on the Chemistry and Uses of Molybdenum" (H. F. Barry and P. C. H. Mitchell, Eds.), p. 224. Climax Molybdenum Co., Ann Arbor, Michigan, 1982.
51. Iannibello, A., Marengo, S., Morelli, G., and Tittarelli, P., *in* "Proceedings, 4th International Conference on the Chemistry and Uses of Molybdenum" (H. F. Barry and P. C. H. Mitchell, Eds.), p. 256. Climax Molybdenum Co., Ann Arbor, Michigan, 1982.
52. Masson, J., Delmon, B., and Nechtschein, J., *C.R. Acad. Sci. Paris* **266,** 428 (1968).
53. Kabe, T., Yamadaya, S., Oba, M., and Miki, Y., *Int. Chem. Eng.* **12,** 366 (1972).
54. Friedman, R. M., Declerck-Grimée, R. I., and Fripiat, J. J., *J. Electron Spectrosc. Relat. Phenom.* **5,** 437 (1974).
55. Ratnasamy, P., Ramaswamy, A. V., Banerjee, K., Sharma, D. K., and Ray, N., *J. Catal.* **38,** 19 (1975).
56. Adamska, B., Haber, J., Janas, J., and Lombarska, D., *Bull. Acad. Pol. Sci. Ser. Sci. Chim.* **23,** 753 (1975).
57. Chiplunker, P., Martinez, N. P., and Mitchell, P. C. H., *Bull. Soc. Chim. Belg.* **90,** 1319 (1981).
58. Clausen, B. S., Topsøe, H., Candia, R., Villadsen, J., Lengeler, B., Als-Nielsen, J., and Christensen, F., *J. Phys. Chem.* **85,** 3868 (1981).
59. Clausen, B. S., Lengeler, B., Candia, R., Als-Nielsen, J., and Topsøe, H., *Bull. Soc. Chim. Belg.* **90,** 1249 (1981).
60. Parham, T. G., and Merrill, R. P., *J. Catal.* **85,** 295 (1984).
61. Dale, J. M., Hulett, L. D., Fuller, E. L., Richards, H. L., and Sherman, R. L., *J. Catal.* **61,** 66 (1980).
62. Ratnasamy, P., Mehrotra, R. P., and Ramaswamy, A. V., *J. Catal.* **32,** 63 (1974).
63. de Beer, V. H. J., Duchet, J. C., and Prins, R., *J. Catal.* **72,** 369 (1981).